This paper must be cited as: Bastos, A. R. N., Brites, C. D. S., Rojas‐Gutierrez, P. A., DeWolf, C., Ferreira, R. A. S., Capobianco, J. A., Carlos, L. D., Thermal Properties of Lipid Bilayers Determined Using Upconversion Nanothermometry. Adv. Funct. Mater. 2019, 29, 1905474. https://doi.org/10.1002/adfm.201905474

Thermal properties of lipid bilayers determined using upconversion nanothermometry

Ana R. N. Bastos, Carlos D. S. Brites, Paola A. Rojas-Gutierrez, Christine DeWolf, Rute A. S. Ferreira, John A. Capobianco,* Luís D. Carlos*

Dr. Ana R. N. Bastos, Dr. Carlos D.S. Brites, Prof. Rute A.S. Ferreira, Prof. Luís D. Carlos
Department of Physics, CICECO - Aveiro Institute of Materials, University of Aveiro, 3810-193, Aveiro, Portugal
E-mail: lcarlos@ua.pt

Paola A. Rojas-Gutierrez, Prof. Christine DeWolf, Prof. John A. Capobianco
Department of Chemistry and Biochemistry, and Centre for NanoScience Research, Concordia University, 7141 Sherbrooke St. West, Montreal, Quebec, H4B 1R6, Canada
E-mail: john.capobianco@concordia.ca

Keywords: luminescence, nanothermometry, upconversion nanoparticle, thermal conductivity, lipid bilayer

Abstract

Luminescent nanomaterials have shown promise for thermal sensing in bio-applications, yet little is known of the role of organic coatings such as supported lipid bilayers on the thermal conductivity between the nanomaterial and its environment. Additionally, since the supported lipid bilayer mimics the cell membrane, its thermal properties are fundamentally important to understand the spatial variations of temperature and heat transfer across membranes. Herein we describe a new approach that enables direct measurement of these thermal properties using a $LiYF_4:Er^{3+}/Yb^{3+}$ upconverting nanoparticle encapsulated within a conformal supported lipid bilayer and dispersed in water as a temperature probe yielding the temperature gradient across the bilayer. The thermal conductivity of lipid bilayer was measured as function of the temperature, being 0.20±0.02 $W \cdot m^{-1} \cdot K^{-1}$ at 300 K. For the uncapped nanoparticles dispersed in water, the temperature dependence of the thermal conductivity was also measured in the 300–314 K range as [0.63–0.69]±0.11 $W \cdot m^{-1} \cdot K^{-1}$. Using a lumped elements model, we calculate the directional heat transfer at each of the system interfaces, namely nanoparticle-bilayer and bilayer-nanofluid, opening a new avenue to understand the membrane biophysical properties as well as the thermal properties of organic and polymer coatings.

Introduction

Temperature is a fundamental intrinsic property of all systems that governs the physical, chemical and biological properties and processes.[1-3] With respect to cellular and molecular biology, temperature can vary between cell types, environments and conditions, and as a result exerts control over cellular processes, biochemical reactions and organization/structure.[4-7]

Fluorescence imaging is a powerful method of intracellular thermometry owing to its high spatiotemporal resolution, and various types of luminescent nanothermometers have recently been developed for this purpose.[8-11] Examples include green fluorescence protein,[12] small

https://doi.org/10.1002/adfm.201905474

organic molecules,[13] quantum dots,[14] polymers[15, 16] and polymer dots[17] and lanthanide-doped nanoparticles.[18-20] Moreover, intracellular temperature mapping has revealed the existence of spatial variations in temperature within single cells.[12-16] However, extreme temperatures are well-known to have adverse impacts on biological systems at both extremes, *i.e.* both hypothermia and hyperthermia. These adverse impacts include cell death which has additionally generated interest in heating as a mode of selectively, eradicating unwanted cell types, for example cancer cells.[21, 22] In addition, several examples of luminescent materials have been proposed for *in vivo* temperature sensing applications, including Ag_2S nanodots to monitor brain thermoregulation,[23] and lanthanide-doped nanoparticles for 2D subcutaneous dynamic thermal imaging.[24] The latter rely on the favorable optical properties of the lanthanide ions which includes the well-described process of upconversion. Upconversion is an anti-Stokes process by which near infrared (NIR) irradiation is converted into Ultraviolet-Visible and NIR emissions. The lanthanide-doped upconverting nanoparticles (UCNPs) present additional properties favorable to temperature sensing that include their resistance to photodegradation, ability to withstand high temperatures, insolubility in water generating stable colloidal solutions and chemical stability (*e.g.* lack of oxidation). In fact, UNCPs have emerged in the last decade as accurate luminescent thermometers[25-29] for diverse applications, such as understanding heat transfer in nanofluids (defined as the colloidal suspension of nanoparticles)[30] and monitoring the reverse quenching process in optoelectronic devices.[31]

Er^{3+} is commonly employed as the dopant for thermal sensing because of the thermally coupled $^2H_{11/2}$ and $^4S_{3/2}$ energy levels. The energy separation between the barycenter of these two states is $\Delta E \sim 700$ cm^{-1}, and, thus, their relative populations are temperature dependent following the Boltzmann distribution. The rate of equilibration of these two states is on the order of 10^{12} s^{-1}, which then dominates over the radiative, non-radiative and energy transfer rates.

https://doi.org/10.1002/adfm.201905474

While different nanomaterials have been proposed for *in vitro* and *in vivo* temperature sensing (as mentioned above), very little is known about the heat transfer properties between the nanoparticle and its cellular or tissue environment. An important question is whether the addition of an organic coating, to functionalize the nanoparticle for biocompatibility, water dispersibility and targeting, impacts its ability to accurately sense the local temperature, specifically if the transfer of heat from the external environment reaches the nanoparticle. If the coating comprises a lipid bilayer, then this also provides valuable information about the transfer of heat across cellular membranes. To date, the thermal conductivity across a lipid bilayer has only been estimated using computational methodologies,[32-34] as the conventional experimental electric methods (*e.g.* the 3ω-method) cannot easily access this property. For example, Youssefian *et al.* used computational methods to show that the thermal resistance was dependent on the temperature gradient across the bilayer, albeit using relatively high temperature gradients up to 68 K.[35]

Wang[33] and Atia[6] highlighted the lack of suitable tools for determining thermal properties at interfaces. Thus, the need to understand heat transfer and accumulation in biological systems, arising from energy inputs to nanodevices, and the mechanisms of thermal management were cited as key questions to be addressed. Frequently the heat transfer is inferred from measurement of bilayer responses but, to our knowledge, were not directly measured or quantified.[34] Herein we describe a new experimental approach that enables direct measurement of the thermal properties of biological membranes using luminescence thermometry. The approach relies on an accurate determination of the thermal gradient across the bilayer which is only possible with the independent measurements of the core temperature inside the bilayer and the external medium temperature. The conformality of the bilayer is essential, as it has been predicted using computational methods that the heat dissipation by structured water between a solid surface and a lipid bilayer increases with the thickness of the water layer.[33] Thus, we

employ $LiYF_4:Er^{3+}/Yb^{3+}$ UCNPs encapsulated within a conformal supported lipid bilayer as luminescent thermal probes in order to calculate the temperature gradient between the particle and the surrounding medium. Moreover, we develop a steady-state temperature model based on the lumped resistance of the components that completely describes the directional heat transfer at each of the system interfaces, namely nanoparticle-bilayer and bilayer-aqueous medium, to determine experimentally the thermal conductivity of the supported lipid bilayer and its temperature dependence between 295 and 315 K. Additionally, the thermal conductivities of the $LiYF_4:Er^{3+}/Yb^{3+}$ core and of the nanofluid with $LiYF_4:Er^{3+}/Yb^{3+}$ UCNPs are calculated. Nanofluids are promising substitutes for conventional liquid coolants, due to a much higher temperature-dependent thermal conductivity (at very low particle concentrations).[36]

Upconverting nanoparticles and lipid bilayer capped upconverting nanoparticles

The oleate-capped $LiYF_4:Er^{3+}/Yb^{3+}$ UCNPs were synthesized using a thermal decomposition method (see Experimental for details) and show a diamond–like morphology with an average size of 86.4±9.5 nm (long diagonal) by 52.2±5.3 nm (short diagonal) with an aspect ratio of 1.7 (**Figure 1**a-c and Table S1 in Supporting Information) obtained from transmission electron microscopy (TEM, Figures S1and S2 in Supporting Information). From the high resolution TEM image, the distance between the lattice fringes was measured to be 4.6 Å, which corresponds to the d-spacing of the (101) planes in the tetragonal $LiYF_4$ structure. $LiYF_4:Er^{3+}/Yb^{3+}$ UCNPs coated with a supported lipid bilayer were prepared using a previously published procedure[37] (see Experimental for details).

The absorption spectra of uncapped UCNPs and lipid bilayer capped UCNPs in water suspension ($1.0\ g{\cdot}L^{-1}$) were measured (Figure S5 in Supporting Information) and the corresponding molar extinction coefficients at 980 nm are determined to be 1.5500±0.0003 and

2.4500±0.0001 $M^{-1}\cdot cm^{-1}$ for the uncapped UCNPs and the lipid bilayer capped UCNPs, respectively (Eq. S1, Supporting information). The absorption cross section was also estimated, yielding values of (1.1600±0.0002)×10^{-21} and (1.1770±0.0008)×10^{-3} nm^2 for the uncapped UCNPs and the lipid bilayer capped UCNPs, respectively (Eq. S2 and S3, Supporting information).

The upconversion emission spectra were recorded in the 298−327 K range upon 980 nm laser excitation (Figure 1d,e). A significant variation in the thermometric parameter Δ, defined as the ratio between the intensity of the $^2H_{11/2}\rightarrow{}^4I_{15/2}$ and $^4S_{13/2}\rightarrow{}^4I_{15/2}$ transitions (Eq. S4 in Supporting Information, Figure 1f), is observed for the uncapped and lipid bilayer capped UCNPs dispersed in H_2O and D_2O (Figures S6 and S11 in Supporting Information). Adopting a strategy reported by some of us previously,[38] the temperature of the suspensions was determined using Δ and Eq. S5 (Supporting Information), knowing ΔE, the intensity ratio in the limit of low excitation power (Δ_0) and the corresponding temperature (T_0). An excellent agreement is observed between the temperature obtained from the immersed thermocouple and that calculated using Eq. S5 (Figure 1g), demonstrating that UCNPs can operate as primary thermometers in all three nanofluids. The relative thermal sensitivity values at 300 K are 1.23, 1.26 and 1.27 $\%K^{-1}$ for the uncapped UCNPs dispersed in H_2O, the lipid bilayer capped UCNPs dispersed in H_2O, and the uncapped UCNPs dispersed in D_2O, respectively. The corresponding temperature uncertainties are 0.26, 0.20 and 0.11 K (Eqs. S5, S6 and details of in Supporting Information Section IV).

Irradiating the nanofluids with NIR radiation (980 nm) we observe a typical transient heating that is recorded by the immersed thermocouple as the temperature increase (ΔT) (**Figure 2a,b**). A dependence of ΔT on the laser power density (P_D), on the presence or absence of a conformal lipid bilayer and on the solvent used is observed. Note that, in this work, we will not discuss the transient regime and will focus on the temperature recorded in the stationary regime. Comparing

the steady-state maximum temperature increase (ΔT_m) recorded for pure water with that of the individual nanofluids it is possible to determine the thermal conductivities of the conformal lipid bilayer and nanofluid (and also their temperature dependences in the 291–315 K interval), and to model the heat transport for distinct heating conditions, as will be detailed below.

Determining the thermal conductivity of the nanofluids

For water, the experimental ΔT_m values were calculated using:[39]

$$\Delta T_m = \frac{\alpha L^2 A_b}{\kappa_w A_s} P_D \quad (1)$$

where α is the absorption coefficient at 980 nm, L is the laser pathlength, A_b is the laser beam spot area, κ_w is the thermal conductivity of water (the particle's surrounding medium), and A_s is the cross-sectional area of the heat flux (see Tables S1 and S2 in Supporting Information).[39] It should be noted that we are assuming that κ_w is constant over the range of the maximal temperature increase (ΔT_m), following the model describing the temperature increment of metallic particles under NIR irradiation.[16, 40] Although there is a small temperature dependence of κ_w (in the temperature increment of Fig. S15, 10 degrees, the variation in κ_w is ~2%, Figure S3, Supporting Information), the experimental results are in a good agreement with the ΔT_m values obtained from Eq. 1 (Figure S15, Supporting Information), indicating that we can rationalize the water heating process in the temperature range investigated using this model.

For the uncapped UCNPs dispersed in D_2O, the observed increase in temperature arises from the UCNPs radiation-to-heat conversion, as D_2O does not absorb significantly at 980 nm.[41] Following the uniform-temperature approximation[40] (Supporting Information, Section V), ΔT_m can be expressed as:

$$\Delta T_m = \frac{N\sigma_{\mathrm{P}}}{4\pi\beta_{\mathrm{P}} r_{\mathrm{P}} \kappa_D} P_{\mathrm{D}} \quad (2)$$

where N is the number of UCNPs exposed to the laser radiation, σ_{P} is the nanoparticle absorption cross-section at 980 nm, β_{P} is the nanoparticle geometrical correction factor due to its faceted structure (Eq. S16, Supporting Information), r_{P} is the equivalent radius of a sphere with the same volume as the nanoparticle, and κ_D is the thermal conductivity of D_2O (particle's surrounding medium). We also assumed κ_D to be constant over the measured temperature range (in the temperature increment of Fig. S15, 4 degrees, the variation in κ_D is ~1%, Figure S4, Supporting Information). Due to the instability of the UCNPs dispersed in D_2O under laser excitation, the measurements were only performed for two laser power densities. Employing the values in Table S2 (Supporting Information), the resulting values predicted using Eq. 2 are in agreement with that obtained experimentally (Figure S15, Supporting Information), evidence that the UCNPs perform as radiation-to-heat converters.

As the water and the nanoparticles can both convert NIR radiation to heat and assuming that both contribute independently to the measured temperature increase, ΔT_{m} for the uncapped UCNPs dispersed in water is expressed by the linear combination of Eq.1 and Eq. 2:

$$\Delta T_m = \frac{1}{\kappa_{\mathrm{f}}}\left(\frac{\alpha L^2 A_{\mathrm{b}}}{A_{\mathrm{s}}} + \frac{N\sigma_{\mathrm{P}}}{4\pi\beta_{\mathrm{P}} r_{\mathrm{P}}}\right) P_{\mathrm{D}} \quad (3)$$

where κ_{f} is the thermal conductivity of the nanofluid (uncapped UCNPs dispersed in water). Using the experimental data of ΔT_{m} *vs.* P_{D} (Figure 2c), κ_{f} was estimated for each P_{D}. A temperature dependence of κ_{f} was observed (Figure 2d), which is typical for aqueous nanofluids.[42] The addition of the uncapped UCNPs (volume fraction of 0.06%) yields approximately an 8% enhancement in the thermal conductivity with respect to water ([0.609–0.638]±0.004 $W \cdot m^{-1} \cdot K^{-1}$, in the temperature range 300–320 K, Figure 2d),[43] in line

with those reported for nanofluids of metallic nanoparticles dispersed in water.[42] The established experimental techniques for determining the thermal conductivity at room temperature and its temperature dependence are contact electrical methods (*e.g.*, transient hot wire and 3-ω methods, respectively)[42, 44] that use complicated experimental setups and data treatment, and are limited to non-conductive nanofluids. The optical method described here, in contrast, allows to easily measure the temperature dependence of the thermal conductivity of the nanofluid, with the advantage of being applicable to virtually any transparent fluid independently of its electrical conductivity.

Determining the thermal conductivity of the lipid bilayer

For the lipid bilayer capped UCNPs dispersed in water, the colloidal suspension temperature increases due to the radiation-to-heat conversion by both the water and the UCNPs (the lipid bilayer does not absorb 980 nm radiation) that are assumed to contribute independently to ΔT_m as described above (Figure 2c). The heat generated by the UCNPs is dissipated to its immediate surrounding medium, which in this case is the lipid bilayer. Thus the thermal conductivity of the lipid bilayer (κ_{L}) must be taken into account and can be estimated using Eq. 4:

$$\Delta T_m = \left[\frac{1}{\kappa_{\mathrm{f}}}\left(\frac{\alpha L^2 A_{\mathrm{b}}}{A_{\mathrm{s}}} + \frac{N\sigma_{\mathrm{L}}}{4\pi\beta_{\mathrm{L}} r_{\mathrm{L}}}\right) + \frac{N\sigma_{\mathrm{P}}}{4\pi\beta_{\mathrm{P}} r_{\mathrm{P}} \kappa_{\mathrm{L}}}\right] P_{\mathrm{D}} \qquad (4)$$

where σ_{L} and β_{L} are the lipid bilayer absorption cross-section and geometrical correction factor (Eq. S17, Supporting Information), respectively, and r_{L} is the radius of a sphere with the same volume as the lipid bilayer. These parameters are given in Tables S1 and S2 in Supporting Information.

In this model, we are assuming that if any heat was to be generated by the lipid bilayer, it would be primarily dissipated through the water, due to the higher lipid bilayer contact surface

area with the water in comparison with that of the UCNP. Therefore, the lipid bilayer contribution in Eq. 4 is divided by the thermal conductivity of the nanofluid (κ_f). In this case, we assume κ_f to be the same as that calculated for the uncapped UCNPs dispersed in water, due to the low contribution of the lipid bilayer in the κ_f value. The heat generated by the UCNPs must be dissipated through the lipid bilayer and, consequently, the UCNP contribution term in Eq. 4 uses the lipid bilayer thermal conductivity. The σ_L value was calculated by subtracting the absorbance values at 980 nm of the two samples (Figure S5), which is equivalent to considering that the absorption difference between the lipid bilayer capped UCNPs and the uncapped UCNP is only due to the conformal lipid bilayer around the nanoparticle. From the experimental data of ΔT_m *vs.* P_D (Figure 2c), and taking into account the temperature dependence of κ_f (Figure 2d), κ_L was estimated for each P_D using Eq. 4. **Figure 3**a shows the thermal conductivity of the lipid bilayer as a function of laser power density used in this study. To the best of our knowledge, this is the first time that the *in-situ* thermal conductivity of a lipid bilayer has been determined experimentally as function of temperature, for which there is an excellent agreement between the experimentally determined value for κ_L and the predicted ones for lipid bilayers.[35, 45]

As observed in Figure 3a, κ_L does not follow a linear relationship with the laser power density, clearly presenting two regimes: (i) for laser power densities lower than 150 $W \cdot cm^{-2}$, the lipid bilayer thermal conductivity decreases, whereas (ii) for laser power densities above 150 $W \cdot cm^{-2}$, it increases. This is due to the marked dependence of κ_L on the temperature gradient across the bilayer that was proposed by Nakano *et al.*[45] based on simulations and determined experimentally (for the first time) in the current work. To understand these results, it is essential to recognize the role of the temperature gradient to which the lipid bilayer is subjected, that can only be accessed by measuring the temperature using both the thermocouple and luminescent thermometer.

https://doi.org/10.1002/adfm.201905474

Understanding the role of the lipid bilayer coating on heat transfer

Figures 2e,f compare the temperature profiles recorded with the immersed thermocouple and that calculated using the emission spectra and Eq. S5 (Supporting Information). Within the experimental uncertainty of both measurements, the values are similar for the uncapped UCNPs dispersed in H_2O (Figure 2e) and D_2O (Figure S16 in Supporting Information). For the lipid bilayer capped UCNPs the values measured by the luminescent thermometer are higher than those of the thermocouple (Figure 2f), showing that the lipid bilayer behaves as a thermal barrier between the UCNP and the water. The temperature difference between the two thermometers depends on the laser power density used: for 150 $W \cdot cm^{-2}$ the temperature difference between the two thermometers is maximized (~1.9 K), and for values higher than 222 $W \cdot cm^{-2}$ it is null within the experimental uncertainty. The temperature gradient across the lipid bilayer $T_P - T_f$, where T_P and T_f are the temperatures of the UCNP's core (measured by the luminescent thermometer) and the nanofluid (measured by the immersed thermocouple), is shown in Figure 3c for laser power densities up to 250 $W \cdot cm^{-2}$.

The two regimes for the κ_L dependence on the laser power density are also discerned in $T_P - T_f$. In regime (i) the lipid bilayer behaves as a thermal barrier, presenting a thermal resistance between the nanoparticle and the water, which leads to increasing temperature gradients (between the two thermometers) with increasing power density. A contributing factor to the ability of the lipid bilayer to serve as a thermal barrier was provided in the computational studies by Nakano,[45] Youssefian,[32] and Potdar,[34] which predicted a discontinuity in heat transfer at the interface between the two bilayer leaflets. In contrast, in regime (ii) the lipid bilayer thermal conductivity increases since it is saturated in the amount of thermal energy it can accept/store and therefore mitigates its ability to serve as a thermal barrier. In the saturation regime, the lipid bilayer allows the heat exchange between the UCNP and the water, eventually leading to no UCNP-water temperature gradient at a power density of 247 $W \cdot cm^{-2}$.

https://doi.org/10.1002/adfm.201905474

Youssefian *et al.* used computational methods to predict that the thermal conductivity would increase at higher temperature gradients due to the increased thermal resistance at the interface of the two bilayer leaflets.[35] At first glance this appear to contrast our results. However, as in their work the temperature gradient was calculated considering the heat flow in the opposite direction of that imposed in the model discussed here the two trends for the temperature dependence of the thermal conductivity are, in fact, consistent.

Additionally, the thermal conductivity of the uncapped UCNPs (κ_P) can also be determined by rationalizing the heat transfer process based on the one-dimensional lumped elements model (Figure 3d).[46, 47] In this model, the UCNPs, lipid bilayer and water are considered as independent heat sources denoted by q_P, q_L and q_f, respectively. The thermal contact resistances are taken as negligible in comparison with the conductive thermal resistances, denoted by R_P, R_L and R_f, for the UCNPs, lipid bilayer and water, respectively, which are given by:

$$R_P = \frac{1}{4\pi\beta_P r_P \kappa_P};\ R_L = \frac{1}{4\pi\beta_L r_L \kappa_L};\ R_f = \frac{L}{A_s \kappa_f}. \quad (5)$$

The heat flow for UCNPs, lipid bilayer and water are given by:

$$q_P = N\sigma_P P_D;\ q_L = N\sigma_L P_D;\ q_f = \alpha L A_b P_D. \quad (6)$$

The heat generated within the UNCPs flows outward, crossing the lipid bilayer to the surrounding medium, water (positive direction). Any heat originating in the lipid bilayer would be divided into a fraction x_1 moving towards the water and the remaining $(1-x_1)$ moving towards the particle's core. Finally, heat released by the water is distributed amongst the bulk water (fraction x_2) and inwards to the lipid bilayer $(1-x_2)$. The values of x_1 and x_2 were calculated using the thermal resistances:

https://doi.org/10.1002/adfm.201905474

$$x_1 = \frac{R_L + R_f}{R_P + R_L + R_f};\ x_2 = \frac{R_f}{R_P + R_L + R_f}\ . \quad (7)$$

Using the lumped elements model, the steady-state temperature gradient across the lipid bilayer $T_P - T_f$ can now be expressed as:

$$T_P - T_f = q_P(R_P + R_L + R_f) + q_L x_1(R_L + R_f) - q_L(1 - x_1)R_P + q_f x_2 R_f - q_f(1 - x_2)(R_P + R_L) \quad (8)$$

Accordingly to this model and to the κ_f and κ_L values estimated before, the UCNP core thermal conductivity (κ_P) was calculated by fitting Eq. 8 with the experimental $T_P - T_f$ values (Figure 3c), yielding to a value of 7.23±0.40 $W \cdot m^{-1} \cdot K^{-1}$ which is in agreement with values known for $LiYF_4$ crystals at room temperature.[48, 49]

Conclusions

Herein we investigated the impact of an organic coating, specifically a supported lipid bilayer, on the ability of the UCNPs to measure temperature. We developed a model to ascertain whether the temperature measured by the nanoparticle using luminescence and that of the surrounding medium using a thermocouple are the same, and to determine the temperature dependence of the thermal conductivity of the lipid bilayer. $LiYF_4:Er^{3+}/Yb^{3+}$ UCNPs encapsulated within a conformal supported lipid bilayer and dispersed in H_2O or D_2O work as primary thermometers with a maximum thermal sensitivity of 1.27 $\%K^{-1}$ and a minimum temperature uncertainty of 0.11 K. For the uncapped UCNPs dispersed in water, the temperature increment induced both by the water and the particles permitted to estimate the temperature

dependence of the nanofluid thermal conductivity, that show a up to ~8% enhancement, relatively to the values of pure water. In the case of uncapped UCNPs, in either H_2O or D_2O, the good agreement between the thermocouple and the luminescent thermometer indicates full thermal equilibrium. On the other hand, in the case of the lipid bilayer capped UCNP, a temperature gradient is observed and found to depend on laser power density. The gradient arises due to both the water and the UCNP acting as independent radiation-to-heat converters. We experimentally determined a lipid bilayer thermal conductivity (0.20 ± 0.02 $W\cdot m^{-1}\cdot K^{-1}$ at 300 K) that decreases as a function of the temperature gradient across the lipid bilayer, which until now has only been predicted using numerical simulations. Furthermore, using a one-dimensional lumped elements model we demonstrate that at low power densities the lipid bilayer can serve as a thermal barrier, limiting the heat transfer between the UCNP and water. However, once a threshold power density (about 150 $W\cdot cm^{-2}$) has been exceeded, the bilayer can no longer serve as a thermal barrier, and the temperature differential between the two thermometers decreases until thermal equilibrium is reached. This must be taken into consideration when using coated nanoparticles for luminescence nanothermometry, especially in biological applications in which the UCNPs are used to measure the intracellular temperature. In such cases, where a coated particle (or an uncapped particle that acquires a protein corona) are used, the luminescent thermometer may not accurately reflect the cell temperature. Moreover, as the supported lipid bilayer mimics the cell membrane, the proposed method to estimate its thermal conductivity and understand its role on heat transfer has significant implications due to the importance of understanding the spatial variations of temperature and heat transfer across membranes.

https://doi.org/10.1002/adfm.201905474

Experimental Section

Materials: Oleate-capped $LiYF_4$ nanoparticles doped with Er^{3+} (0.6%) and Yb^{3+} (29%) $LiYF_4:Er^{3+}/Yb^{3+}$ UCNPs, were synthesized as described previously.[50] The removal of the oleate was achieved via treatment with HCl as described in ref [51]. These uncapped UCNPs are dispersed in either ultrapure water (18.2 MΩ·cm obtained from a Barnstead system) or D_2O (99.9% obtained from Sigma-Aldrich). $LiYF_4:Er^{3+}/Yb^{3+}$ UCNPs coated with a supported lipid bilayer were prepared without removal of the oleate coating using a previously published procedure.[37] The lipids 1,2-di-(9Z-octadecenoyl)-sn-glycero-3-phosphate (DOPA) and 1,2-di-(9Z-octadecenoyl)-sn-glycero-3-phosphocholine (DOPC) were purchased from Avanti Polar Lipids Inc. Cholesterol (99+ %) and all synthetic reagents were purchased from Sigma-Aldrich. The lipid bilayer was prepared in a 64:7:29 DOPA:DOPC:Cholesterol ratio in HEPES buffer. Assuming no loss of oleate, the final bilayer composition was estimated to be Oleate:DOPA:DOPC:Cholesterol (21:51:5:24).[37]

Upconverting nanoparticle structural and chemical characterization: The images of oleate-capped $LiYF_4:Yb^{3+}/Er^{3+}$ UCNPs were collected using a Jeol JEM-2100F microscope operating at 200 keV. The sample was prepared by dropping the nanoparticle dispersion (1.0 g L^{-1} in toluene) onto a 300-mesh Formvar/carbon coated copper grid (3 mm in diameter) followed by evaporation of the solvent. Negative stain images were obtained using a Tecnai 12 Biotwin TEM microscope (FEI Electron Optics) equipped with a Tungsten filament at 120 keV and AMT XR80C CCD Camera System. The sample was prepared by dropping 5 μL of sample solution (1.0 g L^{-1}) onto 200-mesh carbon coated SPI grid and leaving it to be adsorbed during 1 minute before drying it gently with a filter paper. Immediately afterwards, it was stained with 5 μL of 2% uranyl acetate solution and after 1 minute the excess of uranyl acetate solution was removed using a filter paper.

ICP-MS measurements were carried out to determine the nanoparticle concentration after coating the UCNPs with the supported lipid bilayer. The samples were analyzed using an Agilent 7500ce ICP-MS equipped quartz Scott-type spray chamber, an off-axis Omega lens ion focusing, and octopole reaction system with a quadrupole mass spectrometer analyzer operated at 3MHz. Details of the methods can be found in ref [37] and summarized in the Supplementary Information.

Visible-NIR absorption spectroscopy: Visible and NIR absorption spectra were recorded at room temperature, using a dual-beam spectrometer Lambda 950 (Perkin-Elmer) with a 150 mm diameter Spectralon integrating sphere over the range 200-1200 nm with a resolution of 1.0 nm.

https://doi.org/10.1002/adfm.201905474

The baseline was recorded with two 10 mm path-length quartz cuvettes (2 polished windows) containing the reference fluid, H_2O or D_2O. The molar extinction coefficient was estimated from the Lambert-Beer law.

Dynamic temperature measurements: The pure water and the nanofluids were irradiated by a pulsed laser (BrixX 980-1000 HD) at 980 nm with power densities ranging from *ca.* 65 to 250 $W \cdot cm^{-2}$. In the heating regime, the water and the nanofluids were irradiated during 600 s with a pulse frequency of 1.5 MHz, and the consequent temperature increase was measured over time, using an immersed thermocouple (K-type, 0.1 K accuracy) in the water and the nanofluids, and also by upconversion thermometry in the nanofluids. For water, the cooling regime is achieved turned off the pulsed laser and the consequent temperature decrease was measured with the above-mentioned thermocouple. For the nanofluids, however, because the laser is required for the excitation of the nanoparticles the cooling regime was achieved using a much lower pulsed frequency (0.25−0.50 Hz) and a linewidth between 0.100 and 0.250 s, in order to allow the temperature decrease and its measurement using upconversion thermometry and the thermocouple. In both regimes, the emission spectra of the nanofluids were recorded by a portable spectrometer (MAYA Pro 2000, Ocean Optics) with an integration time of 0.500 and 0.250 s, for the nanofluids with the uncapped and lipid bilayer capped UCNPs, respectively. The integration time was chosen in order to maximize the number of recorded spectra, and the spectrum signal-to-noise ratio.

Thermal conductivity: Using the steady-state maximum temperature increase recorded with an immersed thermocouple for each of the individual nanofluids at different laser power densities, the thermal conductivities of the nanofluid and the conformal lipid bilayer were estimated as function of temperature using Eq. 3 and Eq. 4, respectively. Comparing the temperature values measured by the thermocouple and by the luminescent thermometer in the capped UCNPs dispersed in water, and considering the lumped elements model (Eq. 8), the thermal conductivity of the UCNP was estimated.

Supporting Information

Supporting Information is available from the Wiley Online Library or from the author.

Acknowledgements

https://doi.org/10.1002/adfm.201905474

The help of César Vigário and Mengistie Debasu in some of the photoluminescence measurements is gratefully acknowledged. This work has received funding from the European Union's Horizon 2020 FET Open programme under grant agreement Nº 801305 and was partially developed in the scope of the projects CICECO−Aveiro Institute of Materials (FCT UID/CTM/50011/2019), NanoHeatControl (POCI-01-0145-FEDER-031469) and PTDC/CTM-NAN/4647/2014 financed by Portuguese funds through the FCT/MEC and when appropriate co-financed by FEDER under the PT2020 Partnership through European Regional Development Fund in the frame of Operational Competitiveness and Internationalization Programme (POCI). ARNB and CDSB thank the grants financed by the NanoHeatControl and SusPhotoSolutions (CENTRO-01-0145-FEDER-00000) projects, respectively. JAC is a Concordia University Research Chair in Nanoscience and is grateful to Concordia University for financial support. JAC is grateful to the Natural Science and Engineering Research Council (NSERC) of Canada for the sustained support of his research. CDW is grateful to NSERC for support of her research.

Received: ((will be filled in by the editorial staff))

Revised: ((will be filled in by the editorial staff))

Published online: ((will be filled in by the editorial staff))

References

[1] C. D. S. Brites, S. Balabhadra, L. D. Carlos, *Adv. Opt. Mater.* **2019**, *7*, 1801239.

[2] M. Dramićanin, *Luminescence Thermometry: Methods, Materials, and Applications*, Elsevier, Cambridge **2018**.

[3] L. D. Carlos, F. Palacio, *Thermometry at the Nanoscale: Techniques and Selected Applications*, Royal Society of Chemistry, Oxfordshire **2016**.

[4] B. B. Lowell, B. M. Spiegelman, *Nature* **2000**, *404*, 652.

[5] M. H. Guo, Y. F. Xu, M. Gruebele, *Proc. Natl. Acad. Sci. USA* **2012**, *109*, 17863.

[6] L. Atia, S. Givli, *J. R. Soc. Interface* **2014**, *11*, 20131207.

[7] A. I. Ibraimov, *J. Mol. Biol. Res.* **2017**, *7*, 58.

[8] D. Jaque, B. del Rosal, E. M. Rodriguez, L. M. Maestro, P. Haro-Gonzalez, J. G. Solé, *Nanomedicine* **2014**, *9*, 1047.

[9] T. T. Bai, N. Gu, *Small* **2016**, *12*, 4590.

[10] S. Uchiyama, C. Gota, T. Tsuji, N. Inada, *Chem. Commun.* **2017**, *53*, 10976.

[11] K. Okabe, R. Sakaguchi, B. Shi, S. Kiyonaka, *Pflug. Arch. Eur. J. Phy.* **2018**, *470*, 717.

[12] O. A. Savchuk, O. F. Silvestre, R. M. R. Adao, J. B. Nieder, *Sci. Rep.-UK* **2019**, *9*, 7535.

[13] D. Chrétien, P. Bénit, H. H. Ha, S. Keipert, R. El-Khoury, Y. T. Chang, M. Jastroch, H. T. Jacobs, P. Rustin, M. Rak, *PLOS Biol.* **2018**, *16*, e2003992.

[14] R. Tanimoto, T. Hiraiwa, Y. Nakai, Y. Shindo, K. Oka, N. Hiroi, A. Funahashi, *Sci. Rep.-UK* **2016**, *6*, 22071.

[15] K. Okabe, N. Inada, C. Gota, Y. Harada, T. Funatsu, S. Uchiyama, *Nat. Commun.* **2012**, *3*, 705.

[16] X. Q. Chen, Q. Xia, Y. Cao, Q. H. Min, J. R. Zhang, Z. X. Chen, H. Y. Chen, J. J. Zhu, *Nat. Commun.* **2017**, *8*, 1498.

[17] F. M. Ye, C. F. Wu, Y. H. Jin, Y. H. Chan, X. J. Zhang, D. T. Chiu, *J. Am. Chem. Soc.* **2011**, *133*, 8146.

[18] M. Suzuki, V. Tseeb, K. Oyama, S. Ishiwata, *Biophys. J.* **2007**, *92*, L46.

[19] F. Vetrone, R. Naccache, A. Zamarron, Á. J. de la Fuente, F. Sanz-Rodriguez, L. M. Maestro, E. M. Rodriguez, D. Jaque, J. G. Solé, J. A. Capobianco, *ACS Nano* **2010**, *4*, 3254.

[20] R. Piñol, C. D. S. Brites, R. Bustamante, A. Martínez, N. J. O. Silva, J. L. Murillo, R. Cases, J. Carrey, C. Estepa, C. Sosa, F. Palacio, L. D. Carlos, A. Millán, *ACS Nano* **2015**, *9*, 3134.

[21] S. Jain, D. G. Hirst, J. M. O'Sullivan, *Br. J. Radiol.* **2012**, *85*, 101.

[22] G. Baffou, R. Quidant, *Laser Photonics Rev.* **2013**, *7*, 171.

[23] B. del Rosal, D. Ruiz, I. Chaves-Coira, B. H. Juarez, L. Monge, G. S. Hong, N. Fernandez, D. Jaque, *Adv. Funct. Mater.* **2018**, *28*, 1806088.

[24] E. C. Ximendes, U. Rocha, T. O. Sales, N. Fernández, F. Sanz‐Rodríguez, I. R. Martín, C. Jacinto, D. Jaque, *Adv. Funct. Mater.* **2017**, *27*, 1702249.

[25] B. Zhou, B. Shi, D. Jin, X. Liu, *Nat. Nanotechnol.* **2015**, *10*, 924.

[26] M. Bettinelli, L. D. Carlos, X. Liu, *Phys. Today* **2015**, *68*, 38.

[27] G. Y. Chen, H. Agren, T. Y. Ohulchanskyy, P. N. Prasad, *Chem. Soc. Rev.* **2015**, *44*, 1680.

[28] J. Zhou, Q. Liu, W. Feng, Y. Sun, F. Li, *Chem. Rev.* **2015**, *115*, 395.

[29] A. Nadort, J. B. Zhao, E. M. Goldys, *Nanoscale* **2016**, *8*, 13099.

[30] C. D. Brites, X. Xie, M. L. Debasu, X. Qin, R. Chen, W. Huang, J. Rocha, X. Liu, L. D. Carlos, *Nat. Nanotechnol.* **2016**, *11*, 851.

[31] E. D. Martínez, C. D. S. Brites, L. D. Carlos, A. F. García-Flores, R. R. Urbano, C. Rettori, *Adv. Funct. Mater.* **2019**, *29*, 1807758.

[32] S. Youssefian, N. Rahbar, S. Van Dessel, *J. Chem. Phys.* **2018**, *148*, 174901.

[33] Y. Wang, Z. Qin, M. J. Buehler, Z. Xu, *Nat. Commun.* **2016**, *7*, 12854.

[34] D. Potdar, M. Sammalkorpi, *Chem. Phys.* **2015**, *463*, 22.

[35] Y. Sina, R. Nima, L. C. R., V. D. Steven, *J. R. Soc. Interface* **2017**, *14*, 20170127.

[36] R. Saidur, K. Y. Leong, H. A. Mohammad, *Renew. Sust. Energ. Rev.* **2011**, *15*, 1646.

[37] P. A. Rojas-Gutierrez, C. DeWolf, J. A. Capobianco, *Part. Part. Syst. Char.* **2016**, *33*, 865.

[38] S. Balabhadra, M. L. Debasu, C. D. S. Brites, R. A. S. Ferreira, L. D. Carlos, *J. Phys. Chem. C* **2017**, *121*, 13962.

[39] C. D. S. Brites, M. C. Fuertes, P. C. Angelomé, E. D. Martínez, P. P. Lima, G. J. A. A. Soler-Illia, L. D. Carlos, *Nano Lett.* **2017**, *17*, 4746.

[40] G. Baffou, R. Quidant, F. J. García de Abajo, *ACS Nano* **2010**, *4*, 709.

[41] S. Kedenburg, M. Vieweg, T. Gissibl, H. Giessen, *Opt. Mater. Express* **2012**, *2*, 1588.

[42] S. A. Angayarkanni, J. Philip, *Adv. Colloid. Interfac.* **2015**, *225*, 146.

[43] M. L. V. Ramires, C. A. N. d. Castro, Y. Nagasaka, A. Nagashima, M. J. Assael, W. A. Wakeham, *J. Phys. Chem. Ref. Data* **1995**, *24*, 1377.

[44] S. Lee, S. U. S. Choi, S. Li, J. A. Eastman, *J Heat Trans-T Asme* **1999**, *121*, 280.

[45] T. Nakano, G. Kikugawa, T. Ohara, *J. Heat Transfer* **2013**, *135*, 061301.

[46] J. H. L. IV, J. H. L. V, *A Heat Transfer Textbook*, Phlogiston Press, Cambridge, Massachusetts, USA **2003**.

[47] A. Schilling, X. Zhang, O. Bossen, *Sci. Adv.* **2019**, *5*, eaat9953.

[48] R. L. Aggarwal, D. J. Ripin, J. R. Ochoa, T. Y. Fan, *J. Appl. Phys.* **2005**, *98*, 103514.

[49] V. V. Semashko, S. Korableva, A. Nizamutdinov, S. Kuznetsov, P. Popov, A. Baranchikov, K. Nishchev, V. Ivanov, P. Fedorov, *Russ. J. Inorg. Chem.* **2018**, *63*, 433.

[50] V. Mahalingam, F. Vetrone, R. Naccache, A. Speghini, J. A. Capobianco, *Adv. Mater.* **2009**, *21*, 4025.

[51] N. Bogdan, F. Vetrone, G. A. Ozin, J. A. Capobianco, *Nano Lett.* **2011**, *11*, 835.

https://doi.org/10.1002/adfm.201905474

Figures

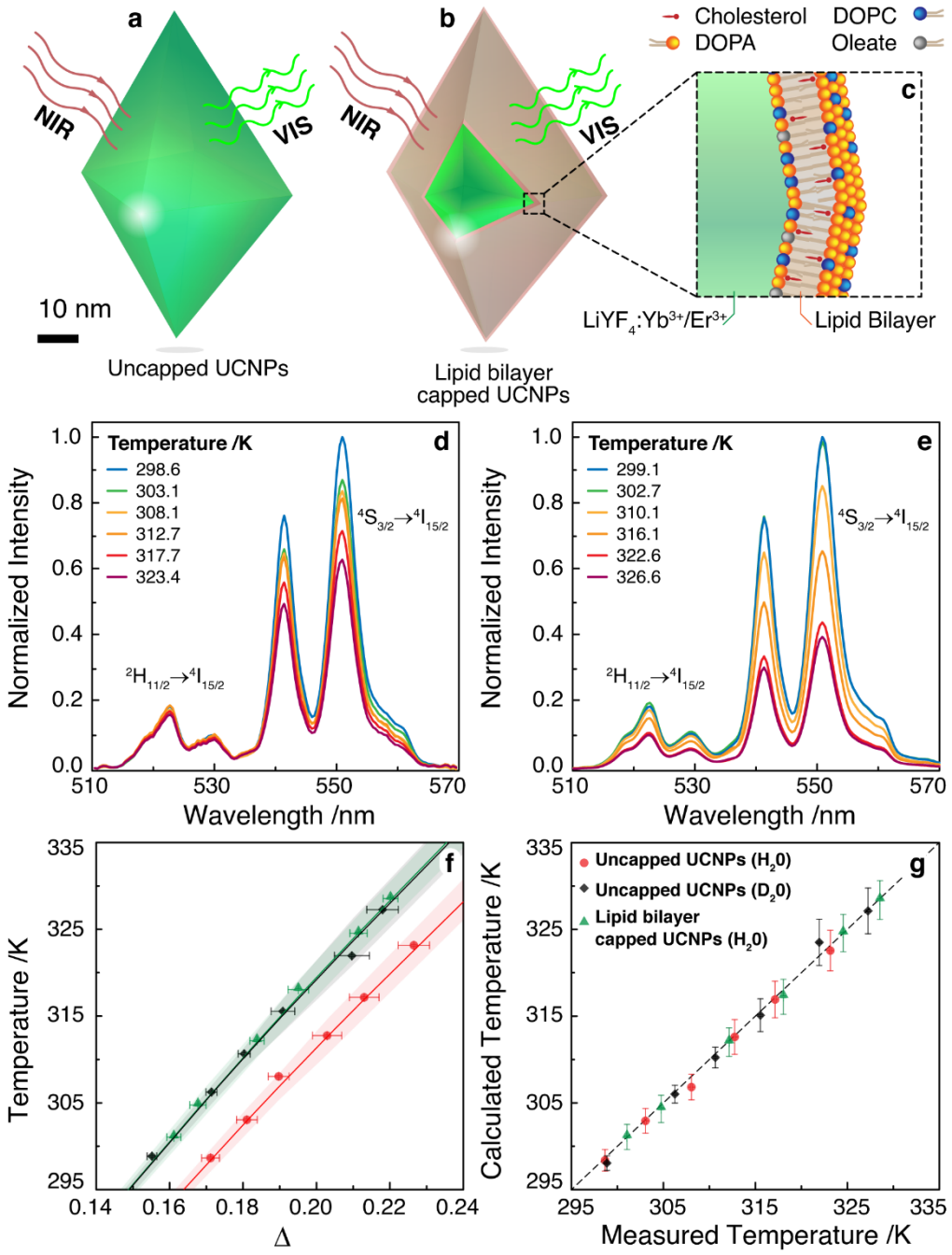

Figure 1. Schematic representation of the **(a)** uncapped and **(b)** lipid bilayer capped $LiYF_4:Er^{3+}/Yb^{3+}$ UCNPs. The magnification **(c)** depicts a simplified one-dimensional model for the lipid bilayer coating. **(d)** and **(e)** Temperature dependent upconverting emission spectra of uncapped and lipid bilayer capped UCNPs dispersed in water, respectively. **(f)** Temperature calibration upon 980 nm irradiation of uncapped UCNPs dispersed in H_2O (red) and D_2O (black), and of lipid bilayer capped UCNPs dispersed in water (green). The solid lines correspond to the temperature calculated using Eq. S5 and the shadowed areas are the corresponding uncertainties. **(g)** Comparison between the temperature determined using Eq.S2 (*y-axis*, calculated temperature) and that measured by an immersed thermocouple (*x-axis*, measured temperature) upon 980 nm irradiation. The line corresponds to $y=x$. In (d), (e), (f), and (g) the 980 nm laser power density is 67 $W \cdot cm^{-2}$.

https://doi.org/10.1002/adfm.201905474

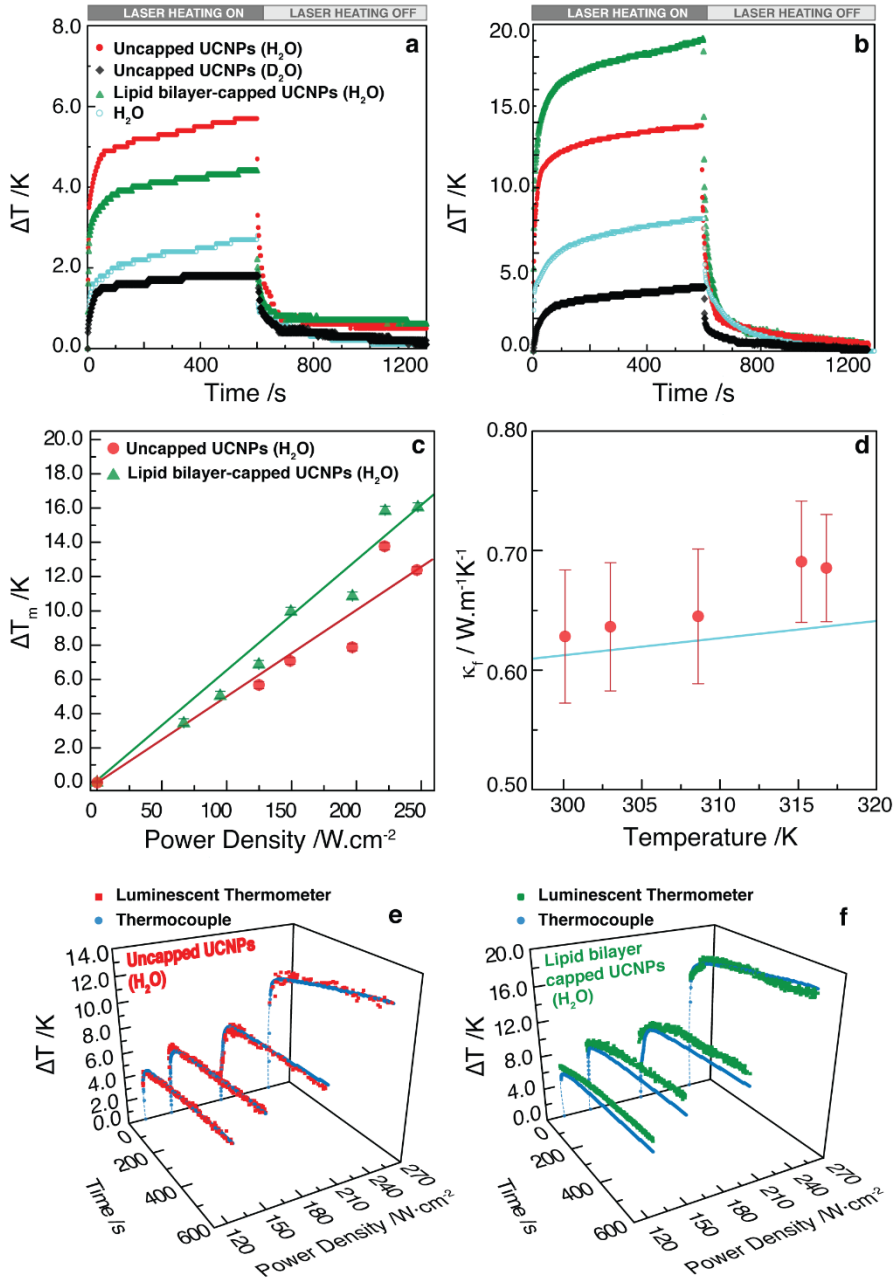

Figure 2. Temperature increase profiles induced by 980 nm laser irradiation at laser power densities of **(a)** 125 and **(b)** 222 W·cm^{-2}, measured by an immersed thermocouple. In the cooling steady-state regime of the two water-based nanofluids the water's absorption of the irradiating laser pulses induces a ~0.5 degree temperature increment. **(c)** Temperature increase induced by laser excitation as function of the laser power density for uncapped UCNPs and lipid bilayer capped UCNPs dispersed in water, measured by the immersed thermocouple. The lines serve as a guide for the eyes only. **(d)** Thermal conductivity of the uncapped UCNPs dispersed in water as a function of temperature. The line corresponds to the standard reference data of the water thermal conductivity.[43] Temperature profiles of the **(e)** uncapped UCNPs and **(f)** lipid bilayer capped UCNPs dispersed in water, measured by the immersed thermocouple (circles) and luminescent thermometer (squares).

https://doi.org/10.1002/adfm.201905474

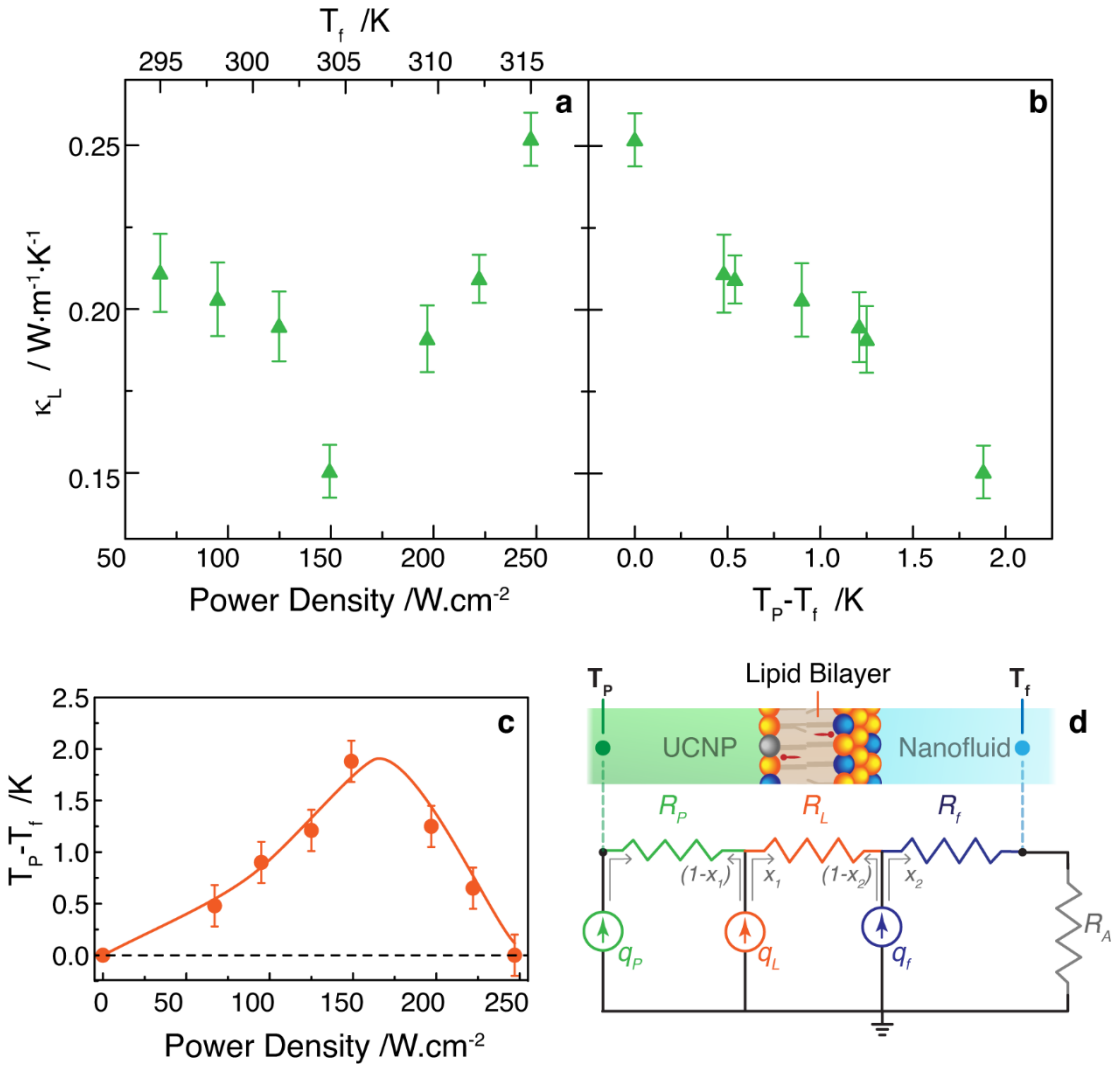

Figure 3. Thermal conductivity of the lipid bilayer as a function of **(a)** laser power density or **(b)** temperature gradient between the upconversion thermometer and the immersed thermocouple at the stationary regime. **(c)** Temperature difference in the stationary regime ($T_P - T_f$) for lipid bilayer capped UCNPs dispersed in water, obtained experimentally (symbols) and calculated using Eq. 8 (line). **(d)** One-dimensional lumped elements of the thermal circuit model for the lipid bilayer capped UCNPs. The ground symbol denotes the reference temperature, and the arrows represent the heat flows. R_A is thermal resistance describing the convective heat transfer from the nanofluid container to the surrounding quiescent air.

https://doi.org/10.1002/adfm.201905474

The thermal properties of organic coatings on inorganic nanoparticles, for example biomimetic lipid bilayers, play a key role in their application as intracellular temperature probes. The measurement of the core temperature using upconversion thermometry enabled direct determination of the bilayer thermal conductivity, opening avenues for studying fundamental membrane biophysical properties and thermal properties of organic and polymer coatings for a wide range of nanomaterials.

Keywords: luminescence, nanothermometry, upconversion nanoparticle, thermal conductivity, lipid bilayer

Ana R. N. Bastos, Carlos D. S. Brites, Paola A. Rojas-Gutierrez, Christine DeWolf, Rute A. S. Ferreira, John A. Capobianco,* Luís D. Carlos*

Thermal properties of lipid bilayers determined using upconversion nanothermometry

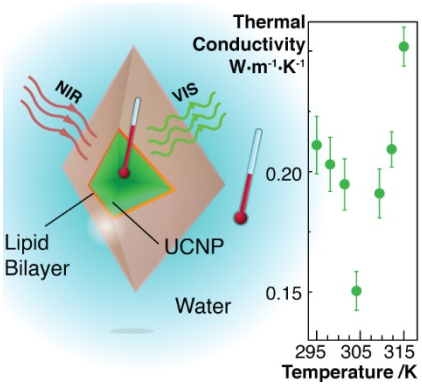

https://doi.org/10.1002/adfm.201905474